Proc. of the European Safety and Reliability Conference (ESREL 2026)
Edited by José C. Matos, Paulo B. Lourenço, Michael Beer, Daniel Oliveira,
Edoardo Patelli, Hélder S. Sousa, Rui A. Silva and Monica Santamaria

doi: 10.3850/ESREL2026061419_esrel26-p26603-cd

Human-Centric Risk Assessment of Metro Systems Under Extreme Rainfall

Hao Bai

College of Civil Engineering, Tongji University; Energy Department, Politecnico di Milano. E-mail: xiaobaihao6666@tongji.edu.cn

Dongming Zhang

College of Civil Engineering, Tongji University. E-mail: 09zhang@tongji.edu.cn

Gang Chen

Shanghai Tunnel Engineering Co., Ltd, E-mail:cgx9000@21cn.com

Enrico Zio

Energy Department, Politecnico di Milano. E-mail: enrico.zio@polimi.it

The process of urbanization and climate change are stressing metro systems, particularly posing risks to passenger safety and mobility. As a complex and interconnected network, the operational status of different components within a metro system is highly interdependent. When a station or tunnel segment is compromised by extreme rainfall (e.g., due to flooding or structural failure), the resulting disruption can propagate throughout the network, impacting passenger flow and travel efficiency. From a human-centric perspective, this study develops a novel risk assessment indicator based on average passenger travel time, integrating the Dynamic Inoperability Input-Output Model (DIIM) with a topological metric of network efficiency. The proposed model dynamically evaluates the degradation of the system performance by analyzing the initial inoperability of affected components and its propagation throughout the network. Taking the Shanghai Metro System as a case study, model parameters are calibrated using historical data, including publicly available ridership records and meteorological data. The analysis reveals the temporal evolution of system performance and identifies key risk propagation pathways under extreme rainfall conditions.

Keywords: Metro System, Extreme Rainfall, Human-Centric Risk Assessment, Dynamic Inoperability Input-Output Model (DIIM), Network Efficiency

1. Introduction

Climate change and rapid urbanization are placing unprecedented stress on metro systems, where extreme rainfall can trigger cascading failures across the interconnected network. When critical components, e.g., stations or tunnels, are disrupted, the impact propagates system-wide, challenging passenger safety and mobility. However, existing risk assessment models are predominantly static and topology-oriented, often failing to capture the temporal evolution of risk and the human-centric experience like actual travel delays. This limitation poses a critical decision-making dilemma for operators: enforcing overly conservative strategies that induce unnecessary disruptions, or underestimating dynamic risks that compromise passenger safety.

To address these gaps, this study proposes a Data-Driven and Simulation-Integrated Dynamic Inoperability Input-Output Model (DIIM). While DIIM is a powerful tool for analyzing risk propagation in Systems of Systems (SoS) (Clavijo Mesa et al. 2025; Bai et al. 2025), its traditional application is hindered by the difficulty of deriving explicit dependency matrices. This research overcomes this by integrating endogenous rainfall and traffic simulations directly into the DIIM framework.

The main contributions of this paper are summarized as follows: (1) A Multilayer Network Model: This paper constructs a coupled network of station and line layers to explicitly map passenger movements. (2) Simulation-Informed DIIM: This paper proposes a modified DIIM where theoretical dependency matrices are replaced by dynamic disturbances computed from multi-source simulation data. (3) Human-Centric Assessment: A "Time-based Network Efficiency" metric is developed. Taking the Shanghai Metro during Typhoon *Co-May* as a case study, this paper quantifies the dynamic system degradation and validate the model against real-world operational adjustments.

2. Methodology

2.1. *Multilayer metro network model*

The metro system in this study is considered as a multilayer network model (Zhang et al. 2025). In this model, the metro system is divided into two parts: one station layer and several line layers, as shown in Fig. 1. The edges between the station layer and the line layers are the paths of the passengers walking through the metro station and boarding the train, namely inter-layer edge. The edges between the nodes in line layers are the paths of passengers traveling from one station platform to another station platform, namely intra-layer edge.

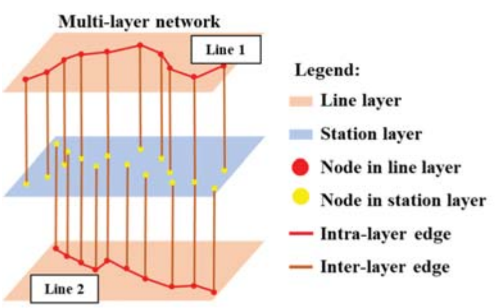

Fig. 1 Multilayer metro network model

2.2. *Data-Driven and Simulation-Integrated DIIM*

The Dynamic Inoperability Input-Output Model (DIIM) provides a robust theoretical framework for characterizing the temporal evolution of system resilience, specifically the propagation of dysfunction and the subsequent recovery process (Clavijo Mesa et al. 2025). The classical DIIM is governed by the equation:

$$q(t+1) = q(t) - k\left[q(t) - A(t)q(t) \text{-} c(t)\right] \quad (1)$$

In this equation, $q(t)$ is the inoperability vector of the system component, and the range of each element in $q(t)$ is [0,1]. The higher the value of $q(t)$, the higher loss of the component. k is the recovery rate coefficient; $kq(t)$ represents the component's own recovery level, and $kA(t)q(t)$ represents the propagation strength of the inoperability of neighboring components to other components. Here, $A(t)$ is the functional dependency matrix, which describes the strength of functional dependency between neighboring components and the component itself; $c(t)$ denotes the disturbance intensity experienced by each component in the system over time.

For metro systems, the DIIM model can also be applied to characterize the propagation of inoperability among components and the self-recovery of components. For example, congestion propagation based on queuing theory indicates that increased train travel time leads to longer passenger waiting times on platforms. On the other hand, due to the emergency management of the metro company, the inoperability of components also undergoes a gradual reduction process.

However, in the context of metro systems under extreme rainfall, the functional dependency matrix $A(t)$ is highly non-linear and state-dependent. For instance, the "dependency" between a station entrance and a platform is not a static coefficient but is physically governed by fluid dynamics or crowd dynamics. Explicitly deriving a closed-form $A(t)$ to capture such complex physical-social coupling is mathematically intractable and often oversimplifies the cascading mechanisms.

To bridge this gap, this study proposes a Simulation-Integrated DIIM framework. Instead of relying on a static or statistically estimated dependency matrix, this study employ endogenous rainfall and traffic simulations to numerically resolve the complex interaction dynamics at each time step. The simulation engine acts as a "state solver," capturing the instantaneous impact of physical disruptions and operational adjustments. These resolved states are then assimilated into the DIIM framework to drive the evolution of inoperability. Consequently, the governing equation is reformulated to integrate the simulation-derived dynamics:

$$q(t+1) = (1-k)q(t) + k\Phi(State_t) \quad (2)$$

Here, $\Phi(State_t)$ is the system state driving function derived from the multi-source simulation. $State_t$

represents the real-time system state vector at time t, including flood levels, passenger accumulation, and train speeds. This hybrid formulation offers two distinct advantages:

1) Capturing Non-linear Dynamics: The function $\Phi(State_t)$ implicitly contains the complex, high-order dependencies that traditional linear matrices $A(t)$ fail to capture, allowing the model to reflect realistic cascading failures such as congestion propagation and flood-induced detours.

2) Governing Recovery Process: By retaining the differential structure of DIIM, specifically the term $kq(t)$, the model preserves the theoretical description of system inertia and recovery. While the simulation Φ drives the disruption based on external shocks, the DIIM framework governs the restoration dynamics based on the recovery coefficient k, ensuring a continuous and mathematically consistent description of the resilience curve.

In this study, the inoperability $q(t)$ is defined on the edges of the multilayer network to align with the passenger travel time metric. The simulation-derived driving term $\Phi(State_t)$ determines the instantaneous inoperability based on the ratio of travel times in disturbed versus normal states. If the edge is an inter-layer edge:

$$q(t) = 1 - \frac{\left(t_{walking} + t_{waiting}\right)_{norm}}{\left(t_{walking} + t_{waiting}\right)_{real}} \quad (3)$$

$(t_{walking}+t_{waiting})_{norm}$ is the walking time and waiting time in the normal state, $(t_{walking}+t_{waiting})_{real}$ is the walking time and waiting time in the real state. If the edge is an intra-layer edge, the inoperability is

$$q(t) = 1 - \frac{\left(t_{riding}\right)_{norm}}{\left(t_{riding}\right)_{real}} \quad (4)$$

$(t_{riding})_{norm}$ is the time passengers riding the train in the normal state，$(t_{riding})_{real}$ is the time passengers riding the train in the real state.

2.3. *Time-based network efficiency*

To address the limitations of existing metro network efficiency models in (Zhang et al. 2025) —specifically the direct summation of inter-layer links (hundreds of meters) and intra-layer links (kilometers) despite their differing orders of magnitude, which fails to adequately quantify the operational impact of external disturbances—this paper proposes a network efficiency metric based on passenger travel time. Compared to conventional network efficiency, the Time-based efficiency better reflects the actual experience of passengers, thereby serving as a more human-centric basis for decision-making. The definition of time-based network efficiency is as follows:

$$E_f = \frac{1}{N_\alpha\left(N_\alpha - 1\right)} \sum_{i,j \in N_\alpha, i \neq j}^{N_\alpha} \frac{1}{\tau_{ij}^{weighted}} \quad (5)$$

Here, $\tau_{ij}^{weighted}$ denotes the minimum weighted travel time incurred by a passenger from the entrance node of the origin station to the exit node of the destination station. The reciprocal, $1/\tau_{ij}^{weighted}$, signifies the passenger flow per unit time along the path, which comprises both intra-layer and inter-layer links. Regarding the inter-layer links,

$$\tau_{n\beta}^{m\alpha} = t_{n\beta}^{m\alpha} \times \frac{1}{w_{n\beta}^{m\alpha}} \quad (6)$$

where $\tau_{n\beta}^{m\alpha}$ represents the weighted time on the link connecting node m in station layer α and node n in line layer β. $t_{n\beta}^{m\alpha}$ denotes the passenger walking and waiting time between these two nodes, while $w_{n\beta}^{m\alpha}$ indicates the passenger flow on the corresponding link. For the intra-layer links,

$$\tau_{v\beta}^{u\beta} = t_{v\beta}^{u\beta} \times \frac{1}{w_{v\beta}^{u\beta}} \quad (7)$$

where $\tau_{v\beta}^{u\beta}$ represents the weighted time on the link connecting node u and node v within line layer β. $t_{v\beta}^{u\beta}$ denotes the in-vehicle travel time between node u and node v in line layer β, while $w_{v\beta}^{u\beta}$ indicates the passenger flow between these two nodes. Referring to (Xu et al. 2024), the paths of passengers are shown in Fig. 2.

The inter-layer links comprise the walking time within the station $t_{walking}$ and the waiting time at the platform $t_{waiting}$. In contrast, the intra-layer links consist of the in-vehicle travel time t_{riding}. Specifically, $t_{walking}$ is significantly influenced by extreme rainfall. For instance, if a station entrance is submerged due to heavy rain, passengers are forced to detour to alternative exits, thereby increasing $t_{walking}$. Additionally, extreme rainfall tends to reduce passenger walking speeds, further contributing to an increase in $t_{walking}$. $t_{waiting}$ depends on the passenger flow volume and the train arrival interval (headway). For example, when the volume of waiting passengers exceeds the carrying capacity of a single train, platform congestion and queuing phenomena occur. t_{riding} is determined by the train operating speed. If tunnel deformation poses a threat to operational safety, or the heavy rain impact the normal operation, trains will actively reduce speed, which in turn leads to extended train arrival intervals.

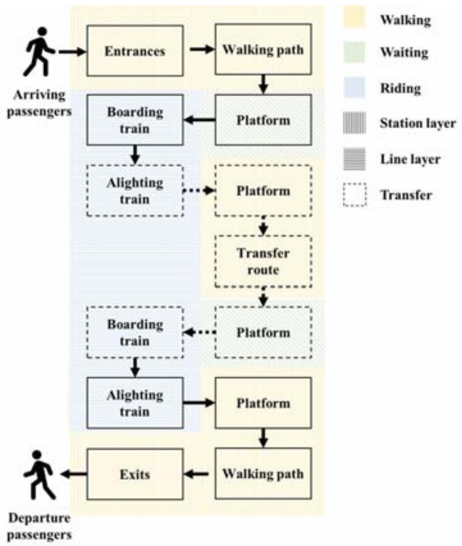

Fig. 2 The paths of passengers in metro systems

3. Case Study

3.1. *Typhoon Co-may in Shanghai*

The Shanghai metro system is selected as the case study for this research. Since its inception in 1995, the network has undergone rapid expansion, playing a pivotal role in the city's socioeconomic development. Currently, the infrastructure spans a total length of 831 km, comprising 20 lines and 508 stations. In terms of ridership, the system handles an annual volume of 2.28 billion passengers, translating to a daily average of 6.40 million trips.

Ridership data for the Shanghai metro network was obtained from the Shanghai Government Data Portal (https://data.sh.gov.cn/). The dataset includes hourly records formatted as (line name, station name, transaction time, inbound volume, outbound volume). In this study, Python was utilized to retrieve JSON data via the platform's API and to conduct subsequent data processing.

Rainfall data for Shanghai was sourced from the Real-time Rainfall Open Data Platform of the Shanghai Water Authority. This platform provides multi-year hourly precipitation records from 886 monitoring stations across Shanghai and its neighboring cities, as shown in Fig. 3. Based on this dataset, spatial interpolation methods were employed to derive rainfall data for specific locations within the city. The drainage simulation is based on the Soil Conservation Service Curve Number (SCS-CN) method (Zhang et al. 2025).

Rainfall intensity values from all weather stations in Shanghai during Typhoon *Co-May* (July 29, 2025 – August 1, 2025, locally referred to as "*Typhoon Zhujiecao*") were utilized to generate hourly spatial distribution maps of precipitation via interpolation techniques, as illustrated in Fig. 4. The figure displays the spatial distribution of rainfall at 6-hour intervals throughout the typhoon event. As observed, precipitation was predominantly concentrated on July 30, 2025, during which major stations across the city were subjected to widespread and intense rainfall.

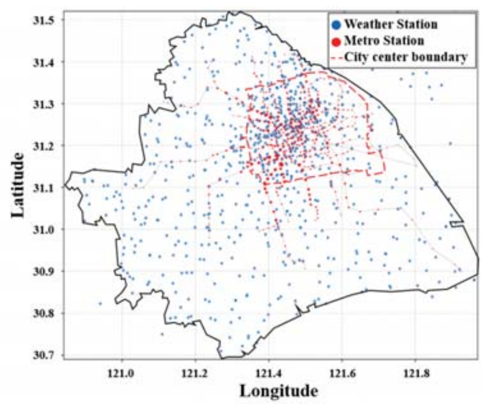

Fig. 3 Rainfall monitoring stations across Shanghai

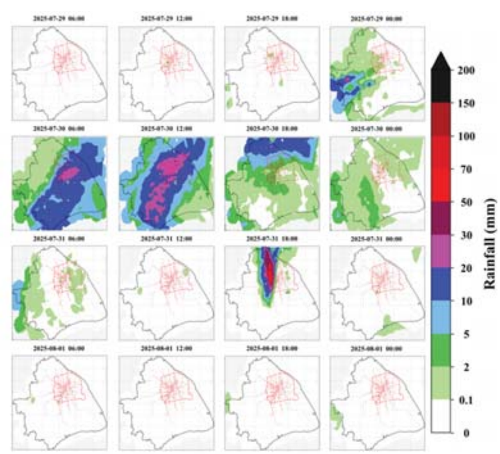

Fig. 4 The rainfall distribution during *Co-May*

To accurately characterize the resilience of the metro system, the recovery rate coefficient k in the DIIM model is calibrated based on the typical recovery time of the network components. We adopt the following logarithmic decay relationship to determine k_i, for each component i:

$$k_i = \frac{1}{T_i}\ln\left(\frac{1}{\varepsilon}\right) \tag{8}$$

where T_i represents the expected recovery time for the component to restore its functionality from a complete failure state to a normal operational level. ε denotes the acceptable threshold of residual inoperability at the end of the recovery period. In this study, ε is set to 0.01, implying a recovery target of 99% availability. Considering the severity of the extreme rainfall event and the complexity of underground drainage, a conservative estimate for the recovery time is adopted, assuming a uniform T_i = 15 hours for all station and line layers. This setting reflects the challenging conditions of pumping out floodwater and conducting safety inspections before resuming full service.

Based on the methodology described previously, the relative network efficiency of the Shanghai metro network was calculated and is presented in Fig. 5. The results indicate that around 06:00 on July 30, coincident with the onset of extreme rainfall, the network efficiency began to degrade, with performance losses propagating rapidly. Although the metro network possesses self-recovery capability, the prolonged duration of the rainfall meant the system remained under persistent perturbation, causing the efficiency to fluctuate at a suppressed level. The minimum of E_f is below 0.6, indicating significant performance degradation of the metro system. The network efficiency only returned to normal levels after the rainfall dissipated. In contrast, a short-duration heavy rainfall event occurred around 18:00 on July 31. While this caused a distinct and sudden drop in network efficiency, with E_f falling below 0.8, the brevity of the rainfall event allowed the system to recover rapidly to its normal operational state.

Due to the confidentiality of real-time operational data (e.g., precise train dispatch logs and passenger tap-in/tap-out records), direct quantitative validation of the simulation results remains a challenge. However, publicly accessible operational logs serve as a reliable ground truth for validating the temporal alignment and magnitude of the system's response. To verify the proposed model, the simulation results was cross-referenced with the official operational notifications released by the Shanghai Metro Authority via their "Weibo" platform during Typhoon *Co-May*, as shown in Table 1.

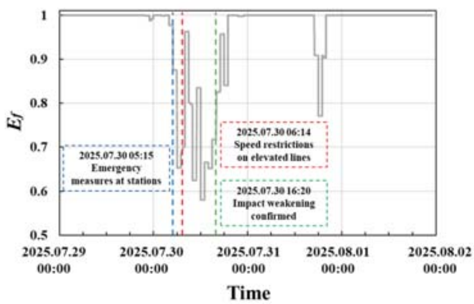

Fig. 5 The relative efficiency of metro system

Table 1 Timeline of operational adjustments by Shanghai Metro during Typhoon *Co-May* (July 30, 2025)

Time	Official notification	Model relevance
04:51	Emergency deployment: Typhoon defense protocols activated.	Enters alert state and initial disturbance starts.
05:15	Station measures: Anti-slip mats laid; water clearing at entrances.	Increases walking time $t_{walking}$.
06:14 - 07:38	Speed restrictions: Limits imposed on Line 16 and parts of Line 2 (above-ground sections).	Increases in-vehicle time t_{riding}; Triggers efficiency drop $E_f < 0.6$.
16:20	Recovery signal: Impact weakening; maintenance scheduled for full recovery.	Marks restoration of recovery rate k_i.

As illustrated in Fig. 5, the simulated network efficiency begins to degrade significantly around 06:00 on July 30. This simulation result aligns remarkably well with the actual timeline of operational interventions. According to the official records, at 05:15, emergency measures such as laying anti-slip mats and clearing accumulated water were actively implemented at stations, which inherently reduced passenger walking speeds $t_{walking}$. Subsequently, at 06:14, the operator officially announced speed restrictions for elevated sections (e.g., Line 16 and parts of Line 2) to ensure safety. These speed limits directly increased the in-vehicle travel time (t_{riding}), corroborating the "suppressed level" of network efficiency observed in our model throughout the day. The simulation shows that efficiency remained low during the rainfall and recovered thereafter; this is consistent with the operator's announcement at 16:20, which confirmed that the impact was weakening and full network recovery was expected by the following day. Although the validation is qualitative, the strong consistency between the simulated performance degradation and the documented real-world operational adjustments, specifically the timing of speed limits and the mechanism of travel time delays, demonstrates that the proposed model effectively captures the dynamic vulnerability of the metro system under extreme rainfall.

3.2. *Influence of rainfall return periods*

To quantitatively analyze other potential risks to the metro system, this study employs the "Chicago Design Storm" (Keifer and Chu 1957) to calculate the design rainfall for urban stormwater infrastructure across different return periods. In this model, the instantaneous rainfall intensity is calculated as follows:

$$i(t_b)=\frac{a\left[\frac{(1-n)t_b}{r}+b\right]}{\left[\left(\frac{t_b}{r}\right)+b\right]^{n+1}} \tag{9}$$

$$i(t_a)=\frac{a\left[\frac{(1-n)t_a}{1-r}+b\right]}{\left[\left(\frac{t_a}{1-r}\right)+b\right]^{n+1}} \tag{10}$$

Where $i(t_b)$ and $i(t_a)$ represent the instantaneous intensities before and after the peak, respectively; t_b and $t_a$denote the rainfall durations before and after the peak;a, b and n are coefficients; and r is the comprehensive peak position coefficient. According to the Shanghai local standard, the Chicago Design Storm is adopted as the design pattern for short-duration rainstorms in Shanghai. The rainfall intensity is expressed as:

$$i(t_b)=\frac{9.581(1+0.846\log P)\left[\frac{(1-0.656)t_b}{r}+7.0\right]}{\left[\left(\frac{t_b}{r}\right)+7.0\right]^{0.656+1}} \tag{11}$$

$$i(t_a)=\frac{9.581(1+0.846\log P)\left[\frac{(1-0.656)t_a}{1-r}+7.0\right]}{\left[\left(\frac{t_a}{1-r}\right)+7.0\right]^{0.656+1}} \tag{12}$$

Where t_b and t_a are measured in minutes; $i(t_b)$ and $i(t_a)$ are in mm/min; and P represents the design storm return period in years. For return periods ranging from 2 to 100 years and rainfall durations under 180 minutes, a unified peak position coefficient of r=0.405 is adopted.

This study utilizes the Areal Reduction Factor (ARF) method to describe the spatial heterogeneity of rainfall distribution in large-scale urban areas. The ARF is defined as the ratio of average rainfall intensity to the point rainfall intensity over a larger area, quantifying the decrease in rainfall intensity as the area of interest increases. In the ARF model, there is a single rainfall center with the highest rainfall intensity per unit area; as the area expands, the ARF value decreases. Referring to (Zhang et al. 2025; He et al. 2025), the rainfall intensity $P(r)$ at a distance r from the rainfall center is calculated as:

$$P(r)=P_0\left[f(r)+\frac{rf'(r)}{2}\right]\left[1+\varepsilon(r)\right] \tag{13}$$

Where $f(r)$ is the reduction factor representing the gradual decrease in rainfall as the area increases, and P_0 is the rainfall intensity per unit area at the rainfall center. Based on historical rainfall data for Shanghai (Tao et al. 2019), the ARF is derived as:

$$f(r)=-0.058\ln\left(\pi r^2\right)+1.0529 \tag{14}$$

Based on the aforementioned methodology, rainfall scenarios with 100-year, 50-year, and 25-year return periods were established. The passenger flow from a rain-free workday (August 8, 2025), close to the Typhoon *Co-May* period, was selected as the baseline passenger flow. The DIIM model was then employed for calculation, with the resulting network efficiency E_f presented in Fig. 6, revealing distinct resilience characteristics across different rainfall intensities. As observed in Fig. 6 (a), under the 100-year return period scenario, the system exhibits a "brittle" failure mode. The network efficiency precipitates from 1.0 to its minimum saturation level (≈0.58$) within a distinctively short time window less than 20 minutes. This rapid degradation implies that under extreme 100-year events, the "time-to-intervention" for metro operators is virtually non-existent, rendering reactive measures like temporary speed restrictions less effective than proactive shutdowns. Conversely, in the 25-year scenario (Fig. 6(c)), the efficiency decline is more gradual, forming a smoother slope. This indicates a progressive accumulation of risk, providing a valuable time buffer for operators to implement dynamic flow control or station-specific evacuations to mitigate further performance loss.

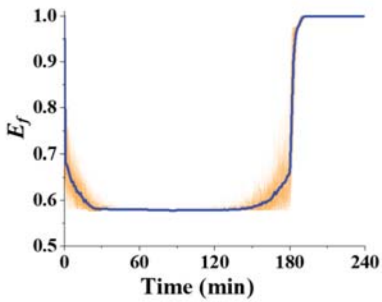

(a) 100-year return period

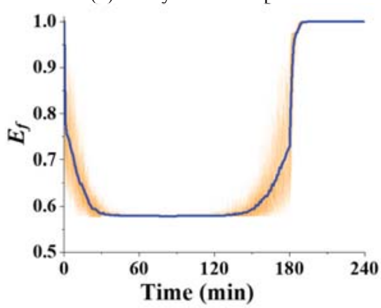

(b) 50-year return period

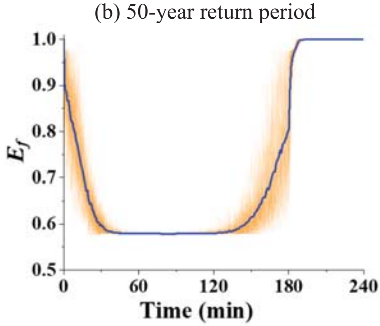

(c) 25-year return period

Fig. 6 Efficiency values of metro network under different rainfall return periods

While the minimum efficiency values across the three scenarios converge to a similar lower bound, dictated by the physical speed limits and maximum flooding depths, the duration of the suppressed state varies significantly. The 100-year scenario traps the system in a low-efficiency state for over 150 minutes, forming a wide "U-shaped" resilience curve. In contrast, the 25-year scenario results in a much narrower trough. This non-linear extension of disruption time with increasing rainfall intensity suggests that the metro system's drainage and recovery capacity face a critical threshold between the 50-year and 100-year levels, beyond which the resilience loss grows exponentially.

The recovery phase also demonstrates intensity-dependent behaviors. For the 25-year and 50-year events, the system shows an elastic recovery, bouncing back to normal operations almost immediately after the rainfall peak passes. However, in the 100-year event, the recovery curve's inflection point is delayed. This suggests that severe flooding induces a "hysteresis effect" in the network—where residual congestion and checking procedures prolong the return to normalcy even after the external disturbance has subsided.

4. Conclusion

This study develops a simulation-integrated DIIM framework to assess metro resilience from a human-centric perspective, overcoming the limitations of static topology metrics. By calculating the "Time-based Network Efficiency," the model effectively quantifies the impact of rainfall-induced delays on passenger experience.

Validated against the Shanghai "Typhoon *Co-May*" event, the model accurately reproduced the system's performance degradation, showing strong temporal alignment with real-world operational adjustments. Sensitivity analysis reveals a non-linear vulnerability: while the network resists frequent disturbances (25-year), 100-year events trigger rapid brittle failures and prolonged recovery hysteresis, identifying critical thresholds for resilience.

Practically, this framework serves as a dynamic decision-support tool, enabling operators to implement precise interventions—such as targeted flow control—rather than relying on binary shutdowns. Future research will extend this approach to address cascading failures across interdependent critical infrastructures like power grids and incorporate granular passenger heterogeneity.

Acknowledgement
This work is substantially supported by National Key R&D Program of China 2024YFC3808804, National Natural Science Foundation of China NO. 52478411, China Scholarship Council No. 202506260003 and Shanghai Tunnel Engineering Co., Ltd (2023-SK-01-5). The financial support is gratefully acknowledged.

References

Bai, Hao, Dong-Ming Zhang, Jian-Min Guo, Yu-Shan Hua, Bilal M. Ayyub, Hong-Wei Huang, Enrico Zio (2025). Resilience of Metro Systems Subjected to External Disturbances: A State-of-the-Art Review. *Resilient Cities and Structures* 4 (4): 72–96. https://doi.org/10.1016/j.rcns.2025.11.002.

Clavijo Mesa, Maria Valentina, Francesco Di Maio, and Enrico Zio (2025). Dynamic Inoperability Input-Output Modeling of a System of Systems Made of Multi-State Interdependent Critical Infrastructures. *Reliability Engineering & System Safety*, 264 December, 111303. https://doi.org/10.1016/j.ress.2025.111303.

He, Renfei, Limao Zhang, and Robert Lk. Tiong (2025). Integrated Location-Inventory Planning of Resource Warehouses for Metro Floods: A Multi-Condition Bilevel Optimization Model. *Reliability Engineering & System Safety*, July, 111498. https://doi.org/10.1016/j.ress.2025.111498.

Keifer, Clint J., and Henry Hsien Chu. (1957). Synthetic Storm Pattern for Drainage Design. *Journal of the Hydraulics Division* 83 (4): 1332–25. https://doi.org/10.1061/JYCEAJ.0000104.

Tao, Xiancheng, Xin Zhang, and Xiqing Wang (2019). Analysis on Characteristics of Rainfall Distribution in Shanghai. *Water Purification Technology* 38 (10): 25–28. https://doi.org/10.15890/j.cnki.isjs.2019.10.005.

Xu, Peng-Cheng, Qing-Chang Lu, Tao Feng, Jing Li, Gen Li, and Xin Xu (2024). Resilience Analysis of Metro Stations Integrating Infrastructures and Passengers. *Reliability Engineering & System Safety*, 252 December: 110467. https://doi.org/10.1016/j.ress.2024.110467.

Zhang, Dong-Ming, Hao Bai, Can-Zheng Zheng, Hong-Wei Huang, Bilal M. Ayyub, and Wen-Jun Cao (2025). Extreme Rainfall Induced Risk Mapping for Metro Transit Systems: Shanghai Metro Network as a Case. *Reliability Engineering & System Safety*, 262 October: 111234. https://doi.org/10.1016/j.ress.2025.111234.